

# Exploring nonequilibrium Andreev resonances in ultraclean graphene Andreev interferometers

Asmaul Smitha Rashid,<sup>1,2</sup> Le Yi,<sup>3,2</sup> Takashi Taniguchi,<sup>4</sup> Kenji Watanabe,<sup>5</sup> Nitin Samarth,<sup>3,6,2</sup> Régis Mélin,<sup>7</sup> and Morteza Kayyalha<sup>1,2,\*</sup>

<sup>1</sup>*Department of Electrical Engineering, The Pennsylvania State University, University Park, Pennsylvania 16802, USA*

<sup>2</sup>*Materials Research Institute, The Pennsylvania State University, University Park, Pennsylvania 16802, USA*

<sup>3</sup>*Department of Physics, The Pennsylvania State University, University Park, Pennsylvania 16802, USA*

<sup>4</sup>*International Center for Materials, Nanoarchitectonics,*

*National Institute for Materials Science, 1-1 Namiki, Tsukuba 305-0044, Japan.*

<sup>5</sup>*Research Center for Functional Materials, Institute for Materials Science, 1-1 Namiki, Tsukuba 305-0044, Japan*

<sup>6</sup>*Department of Materials Science and Engineering,*

*The Pennsylvania State University, University Park, Pennsylvania 16802, USA*

<sup>7</sup>*Université Grenoble-Alpes, CNRS, Grenoble INP, Institut NEEL, Grenoble, France*

(Dated: May 16, 2024)

We study nonequilibrium Andreev resonances in a voltage-biased graphene three-terminal Josephson junction (JJ). We observe periodic oscillations of resistance with maxima at multiples of the magnetic flux quantum (noninversion regime). As we increase the bias voltage, we further observe a transition point beyond which oscillations exhibit a  $\pi$  phase shift (inversion regime) with maxima of resistance occurring at multiples of half-flux quantum. At this transition point, the frequency of the oscillations is doubled. We develop a model based on the coupling of the static Andreev bound states (ABSs) to the nonequilibrium Fermi surface of graphene to explain the observed noninversion to inversion crossovers. Our model associates these crossovers to microscopic phase-sensitive Andreev reflections which couple the normal and superfluid components of the current. Our findings show that multiterminal JJs can be used to engineer unconventional energy-phase relations such as those expected in the  $\pi$ -shifted ABSs without relying on quartet and Floquet physics. These nonequilibrium ABSs could potentially find applications in superconducting  $\pi$  qubits.

At a normal-superconductor interface (NS), Andreev reflections (ARs) occur where an electron retroreflects as a hole, transmitting a Cooper pair into the superconductor. In SNS junctions, two NS boundaries act as AR mirrors and the spatially varying order parameter leads to the formation of Andreev bound states (ABSs) at energies below the superconducting gap [1–4]. The ABS spectrum in an SNS junction depends on the phase difference between the two superconductors [5] and has been exploited for applications that include ABS qubits at a point contact [6], superconducting spin qubits [7, 8], and Andreev quantum dot qubits [9]. The coupling of SNS junctions to electromagnetic (EM) fields [10] or quasi-particle currents [11] opens avenues to the study of nonequilibrium quantum systems based on ABSs. This has led to experimental investigations of nonequilibrium physics involving the interplay between Zeeman splitting and spin-orbit coupling in ABSs [12], Floquet-Andreev states [13, 14], and photon-assisted tunneling processes in hybrid JJs [15]. In this context, hybrid device geometries that combine SNS junctions with proximal normal metal channels, specifically in cross-like hybrid structures, have also been investigated for engineering  $\pi$  and  $\Phi_0$  junctions [16–18]. However, it is challenging to elucidate the mechanisms underlying nonequilibrium ABSs via EM irradiation and normal-current injection techniques because of non-uniform coupling and heating effects [10, 11, 13].

Multiterminal Josephson junctions (MTJJs) have recently emerged as an alternative platform for the investigation of ABSs in the absence of EM irradiation but in the presence of voltage biasing, which we refer to as nonequilibrium Andreev resonances. MTJJs consist of multiple ( $n \geq 3$ ) superconducting terminals coupled to each other through a normal scattering region. The resulting ABSs depend on  $n - 1 \geq 2$  superconducting phase differences and are predicted to host exotic phenomena such as topological phases and Weyl singularities [19–24], quartet Cooper pairs [25, 26], and Floquet-Andreev bands [27–30]. Moreover, voltage-biased MTJJs provide an attractive playground for the exploration of nonequilibrium ABSs [31]. In this case, the applied bias voltage creates a time-dependent superconducting phase difference with a frequency of  $2eV/\hbar$  where  $e$  is the electron charge,  $\hbar$  is the reduced Planck’s constant, and  $V$  is the voltage across the junction. In a manner analogous to an RF source, the voltage bias triggers a transition to a nonadiabatic regime, resulting in the emergence of nonequilibrium ABSs at higher energy levels.

Experimental studies of MTJJs have so far focused on the DC characteristics [32–35], the inverse AC Josephson effect [36], topological phases [37], quartet physics [38–43], hybridization of Andreev modes [44–47], superconducting spin and parity manipulation [48], and non-reciprocal superconducting transport [49–53]. A recent experiment has also explored nonequilibrium ABSs in Cooper quartets in a four-terminal graphene JJ. This study reports a zero to  $\pi$  crossover of differential conduc-

\* Corresponding author: mzk463@psu.edu

tance  $G$  versus superconducting phase  $\varphi$  [54] and associates it with possible Floquet-ABSs. Here, the crossover is primarily a property of the quartet critical current  $I_q \propto \sin \varphi_q$ , where  $\varphi_q$  is the gauge-invariant quartet phase. In addition to experimental studies, several theoretical models including zero-dimensional Floquet theory in quantum dots [55], split quartets arising from perturbation theory [56], interplay between the Josephson and Aharonov-Bohm effects in Andreev interferometers [16] have been considered to understand the dynamics of nonequilibrium ABSs. Despite all the progress, however, the emergent nonequilibrium ABSs and their relationship with the superconducting condensate have not yet been fully understood experimentally. Moreover, in a two-fluid picture, the friction between the normal and superfluid components of the current is theoretically predicted to host non-trivial current-phase relations under nonequilibrium conditions [57]. This friction and the resulting nontrivial CPRs, however, have not been thoroughly explored in experiments.

In this paper, we design an Andreev interferometer based on graphene three-terminal JJs to experimentally investigate the interplay between the nonequilibrium Fermi surface of graphene and the superconducting condensate by controlling superconducting phases and voltage biases. Our interferometer produces periodic oscillations of resistance ( $R$ ) with respect to the superconducting phase difference ( $\varphi$ ). We refer to this regime as “noninversion,” where the oscillations exhibit maxima at multiples of the magnetic flux quantum. As we increase the bias voltage, we observe a doubling of the frequency followed by a  $\pi$  shift in the  $R$  versus  $\varphi$  oscillations. We refer to this regime as “inversion,” where the oscillations exhibit maxima at multiples of half flux quantum. We observe multiple inversion-noninversion crossovers with increasing the bias voltage.

To interpret our results, we develop a model based on the interplay between the static ABSs and the nonequilibrium Fermi surface of graphene [58]. We calculate an energy spectrum for the ABSs that follows that of long junctions [1–4]. As the chemical potential increases with the bias voltage, we find that it crosses the spectrum of higher-energy ABSs resulting in the emergence of noninversion and inversion resonances at multiples of flux and half flux quantum, respectively. At a microscopic level, our model attributes the inversion resonances to a phase-sensitive Andreev reflection (phase-AR) process in which a spin-up electron is coherently transferred through the static ABSs and is then converted to a spin-down electron in the graphene region. In this case, the exchange of an unpaired electron with a Cooper pair results in a  $\pi$  shift in the energy-phase relation of the ABSs. Furthermore, compared to SNS junctions with normal contacts [59, 60], we find that ABSs have longer lifetime and smaller linewidth broadening. This longer lifetime is facilitated by the superconducting gaps which protect ABSs against the short relaxation time of the quasiparticle continua. The enhanced ABS lifetime further ex-

plains the observation of several inversion-noninversion crossovers in our experiments (see more details about this model in Ref. [58]). We finally conclude that the crossovers are a generic response of voltage-biased MTJJs without the need to invoke quartet or Floquet physics. We speculate that our study of nonequilibrium ABSs is potentially useful for practical applications in quantum systems such as voltage-tunable  $\pi$  junctions, cryogenic memories, and superconducting  $\pi$  qubits [61–63].

We fabricate Andreev interferometers on hBN/graphene/hBN van der Waals heterostructures that are edge-contacted by Ti (10 nm)/Al (80 nm) superconducting electrodes [64]. The graphene channel in the device is 1  $\mu\text{m}$  long and 0.5  $\mu\text{m}$  wide. Figure 1A shows a scanning electron microscope (SEM) image of a representative three-terminal Andreev interferometer. The left, right, and top terminals are denoted as  $S_L$ ,  $S_R$ , and  $S_T$ , respectively. Furthermore, terminals  $S_R$  and  $S_T$  in this geometry are connected by a superconducting (SC) loop. This loop allows us to control the superconducting phase between the  $S_R$  and  $S_T$  terminals via an external magnetic flux as  $\varphi = 2\pi\Phi/\Phi_0$ , where  $\varphi$  is the superconducting phase,  $\Phi$  is the magnetic flux, and  $\Phi_0 = h/2e$  is the flux quantum. We apply current  $I_{dc}$  to the terminal  $S_L$  and measure the voltage  $V_{LT}$  between  $S_L$  and  $S_T$ . As a result, the three-terminal Andreev interferometer ( $S_L, S_R, S_T$ ) is at  $(V_{LT}, 0, 0)$  bias voltage configuration. We note that the Al tunneling probe in this device exhibits resistance in the order of tens of  $\text{M}\Omega$  and hence does not play any role in the transport properties of our Andreev interferometer; see results for another device without any tunneling probe in the supporting information (SI). To reduce Joule heating, we perform all the measurements at 300 mK if not otherwise specified [65].

We select graphene as a material of choice for our experiments because graphene offers ballistic transport, supports transparent superconducting contacts, and allows gate tunability of the superconducting coupling [66, 67]. We design our device such that all the terminals are uniformly connected to the graphene channel, i.e., the distance between each pair of terminals from the graphene center is the same ( $\sim 0.5 \mu\text{m}$ ); see Fig 1A. Furthermore, we fabricate the graphene channel such that no independent two-terminal JJ is formed between the neighboring terminals. This design prevents the formation of a circuit network of independent two-terminal JJs and establishes the connection between superconducting terminals via a common scattering region (graphene) [49].

To investigate the interplay between ABSs and the nonequilibrium Fermi surface of graphene, we first explore the critical current modulation as a function of the superconducting phase in our three-terminal Andreev interferometers. Figures 1B and C show the color plot of the differential resistance  $R$  as a function of the magnetic field  $B$  and, respectively, the bias voltage  $V_{LT}$  and the bias current  $I_{dc}$  at the gate voltage  $V_g = 0$  V. The dark

blue region corresponds to the supercurrent with  $R = 0$ . We observe modulations of the supercurrent as a function of the magnetic flux. The period of the modulations is approximately  $\Delta B = 0.8$  G which is consistent with  $\Delta B = 0.827$  G, corresponding to one flux quantum for the enclosed superconducting loop area of  $25 \mu\text{m}^2$ . We further observe a series of dark-bright regions (indicated by arrows) appearing outside of the superconducting region. To better illustrate these regions, we plot line cuts of  $R$  versus  $\Phi/\Phi_0$  (corresponding to the red arrow in Figures 1B and C) at various  $V_{LT}$ 's in Fig. 1D. For  $V_{LT} < -35 \mu\text{V}$ , we observe resistance oscillations at multiples of the flux quantum ( $k\Phi_0$ , where  $k$  is an integer) with a periodicity of  $\Phi_0$ . We refer to this regime as noninversion. As we increase the bias voltage, we observe a doubling of the frequency of oscillations at  $V_{LT} \approx -35 \mu\text{V}$ , highlighting a transition point. Beyond this transition point, we observe  $\pi$ -phase shifted oscillations, i.e., the maxima of resistance occur at multiples of half flux quantum, i.e.,  $(2k+1)\Phi_0/2$ , where  $k$  is an integer. Thus, changing the bias voltage produces noninversion to inversion crossovers in  $R$  versus  $\varphi$ . In total, we observe four crossovers for bias voltages  $V_{LT} < \Delta = 180 \mu\text{eV}$ , where  $\Delta$  is the superconducting gap of Aluminum; see the SI for line cuts corresponding to purple, yellow, and black arrows in Figs. 1B and C. We further note that the crossovers primarily emerge at small bias voltages ( $V_{LT} \leq 45 \mu\text{eV}$ ) where the contribution from multiple Andreev reflections is negligible; see the SI for colormaps of the resistance at various temperatures.

To better elucidate the underlying mechanism giving rise to the crossovers, we introduce a phase-sensitive AR process in our three-terminal Andreev interferometers. Figure 2A shows the schematics of this phase-Andreev reflection process in a voltage-biased three-terminal Andreev interferometer. When  $S_L$  is at zero bias voltage ( $V_{LT} = 0$  V), Cooper pairs transmit between  $S_L$  and ( $S_R$ ,  $S_T$ ) via static ABSs resulting in a DC Josephson current proportional to  $\sin \Phi$ . In contrast, when  $V_{LT} \neq 0$  V, a spin-up electron is Andreev reflected at the  $N - S_R$  interface and the resulting spin-down hole is coherently transferred through the ABSs to the  $N - S_T$  interface, where it is Andreev reflected into a spin-up electron. This AR process is phase sensitive and the resulting ABSs are coupled to the density of states (DOS) of graphene as denoted by the wavy line ( $\rho$ ) in Fig. 2A. The microscopic process of phase-AR produces a current flow from  $S_L$  to ground that couples to the supercurrent in the loop [58].

We consider the device structure of Fig. 1A with superconducting phase variables  $\varphi_R \simeq \varphi_0 + \Phi/2$  and  $\varphi_T \simeq \varphi_0 - \Phi/2$ , where  $\varphi_0$  is the independent phase variable and  $\Phi$  is the external magnetic flux threading the loop. In this case, the phase variable  $\varphi_R - \varphi_T \simeq \Phi$  is the only static variable in our calculations. In other words, other phase variables, e.g.,  $\varphi_{R,T} - \varphi_L$ , have AC components when  $V_{LT} \neq 0$ . We note that our three-terminal Andreev interferometer operates in the AR regime for  $V_{LT} \neq 0$ , and any DC transport of Cooper pairs is absent from  $S_L$

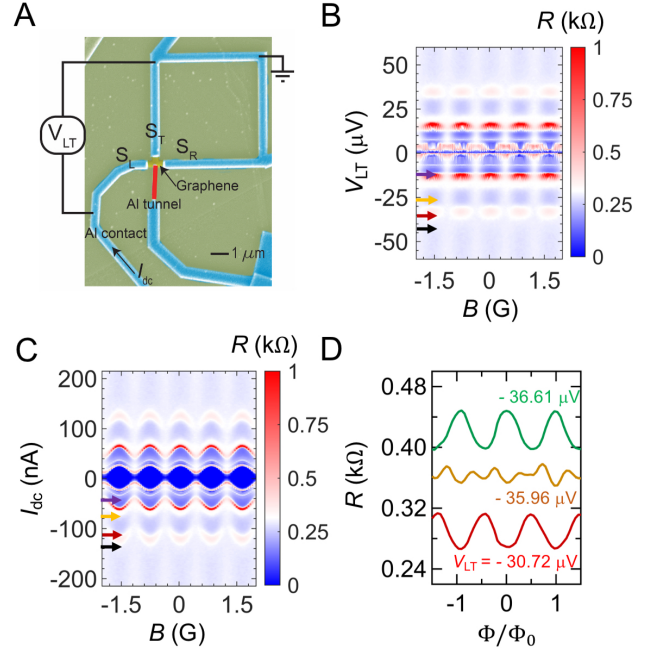


FIG. 1. (A) Scanning electron microscope (SEM) image of a representative three-terminal Andreev interferometer along with the measurement configuration. Current  $I_{dc}$  is applied to terminal  $S_L$  and voltage  $V_{LT}$  is measured between terminals  $L$  and  $B$ . The superconducting loop (SC) is grounded. (B, C) Differential resistance  $R$  as a function of the magnetic field  $B$  and  $V_{LT}$  (B) and bias current  $I_{dc}$  (C). Arrows mark noninversion to inversion crossovers. (D) Differential resistance  $R$  as a function of the magnetic flux  $\Phi$  for the crossovers marked by the red arrows in (B) and (C). The oscillations show an evolution from maxima to minima with increasing  $V_{LT}$ . Curves are shifted vertically by  $0.03 \text{ k}\Omega$  for clarity. Colormaps are saturated to better highlight noninversion to inversion crossovers. These maps are generated by sweeping  $B$  and  $I_{dc}$  with step sizes of  $0.05 \text{ G}$  and  $1 \text{ nA}$ , respectively.

to  $S_R$  and  $S_T$ . Instead, we have AC Josephson oscillations of the current flowing from  $S_L$  to  $S_R$  and  $S_T$ . The dissipative component of this current results in a change of the chemical potential by  $\delta\mu_N = eV_{LT}$ , which in turn leads to voltage sensitive jumps in the nonequilibrium distribution function of graphene [58].

Figure 2B schematically shows the spectrum of the nonequilibrium ABSs arising from the voltage sensitive jumps in the chemical potential. These ABSs resemble those expected in the long-junction limit [2–4]. Our model predicts that the chemical potential  $\mu_N$  (dash horizontal lines) increases with increasing  $V_{LT}$  and eventually crosses the spectrum of ABSs at higher energy ABSs when  $E(\varphi_T - \varphi_R) = \mu_N$ . The high-energy ABSs exhibit  $\pi$ -shifted energy-phase relation, thereby resulting in the observation of  $\pi$ -shifted (inversion) resonances in  $R$  versus  $\varphi$ . Alternating between different spectra of ABSs via further increase of  $\mu_N$  will yield crossovers between resonances with maxima at multiples of flux quantum (red curves) and half flux quantum (blue curves), which we



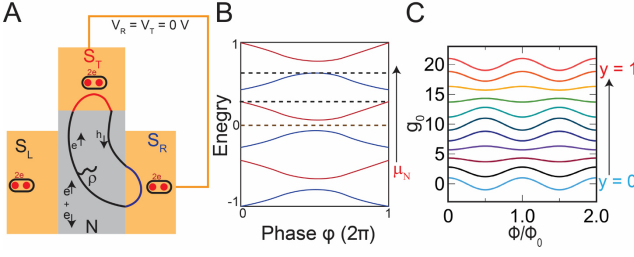


FIG. 2. (A) Schematics of the phase-Andreev reflection (AR) process in a three-terminal Andreev interferometer where the wavy line represents coupling to the density of state in the normal region, via the nonlocal Keldysh Green's function. (B) The schematic diagram of energy versus phase relation of nonequilibrium Andreev bound states (ABSs). The dashed lines mark the chemical potential  $\mu_N$  which changes with  $V_{LT}$ . (C) Theoretically calculated dimensionless conductance  $g_0$  as a function of  $\Phi/\Phi_0$  at various effective Fermi energies ( $y$ 's).

refer to as noninversion to inversion crossovers.

To calculate the differential conductance of the graphene Andreev interferometer, we assume an infinite planar geometry. We further assume the normal-superconductor interferometer to be uniform in space with no geometrical resonance. We calculate the current  $I_{LT}$  defined by Keldysh Green's functions and obtain the differential conductance  $dI_{LT}/dV_{LT}$  within the lowest order perturbation theory as a function of bias voltage  $V_{LT}$  and current  $I_{LT}$ . We obtain a dimensionless conductance ( $g_0 \propto dI_{LT}/dV_{LT}$ ) where  $g_0(\Phi/2\pi, V_{LT}R/\pi\hbar v_F) = \cos\Phi \cos(2eV_{LT}R/\hbar v_F)$ . We note that unlike Ref. [54] where the quartet critical current ( $I_q \propto \sin\varphi_q$ ) is responsible for crossovers, in our system, the conductance is proportional to  $\cos\Phi$  instead of the expected  $\sin\Phi$  for the equilibrium DC Josephson current between  $S_T$  and  $S_R$ . This  $\cos\Phi$  term is physically controlled by the friction between the normal and superfluid components of the current, and realizes the Andreev mechanism of conversion between the normal current and supercurrent.

We also find ballistic undamped oscillations in conductance as  $\cos(2eV_{LT}R/\hbar v_F)$  where  $E = eV_{LT}$  is the bias voltage energy,  $\tau = R/v_F$  is the ballistic propagation delay between  $S_R$  and  $S_T$ , and  $v_F$  is the Fermi velocity. These undamped oscillations in the conductance contrast with the damping predicted in the diffusive limit [68]. Figure 2C plots the calculated  $g_0$  as a function of  $\Phi/\Phi_0$  and effective Fermi energy  $y = V_{LT}R/\pi\hbar v_F$ . We observe multiple noninversion to inversion crossovers with increasing bias voltage  $V_{LT}$  in this theoretical plot, corroborating the experimental findings in Figs. 1B-D. Finally, we find theoretically that the line width broadening of ABSs is reduced by a factor of  $\eta_s/\Delta$ , where  $\eta_s$  is Dynes parameter, if a superconducting terminal  $S_L$  is used instead of a normal contact in the Andreev interferometer. The emergence of a long timescale and small linewidth broadening points to the protection of the ABSs against the short relaxation time of the quasiparticle continua; see more details about our calculations in ref. [58].

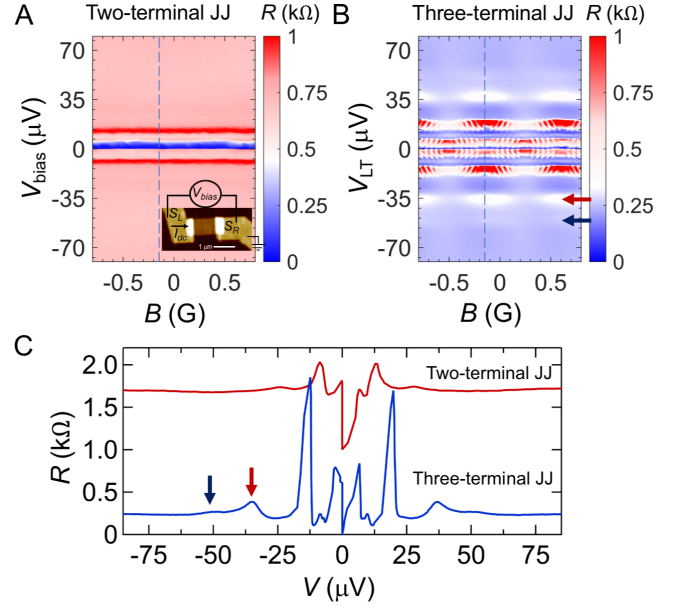


FIG. 3. (A-B) Differential resistance  $R$  as a function of  $B$  and the bias voltage  $V_{bias}$  in a two-terminal JJ (A) and  $V_{LT}$  in a three-terminal Andreev interferometer (B). Inset in A shows the atomic force microscope (AFM) image of the two-terminal JJ alongside the measurement configuration. (C) Line cuts of  $R$  versus  $V$  for two-terminal JJ (red) and three-terminal Andreev interferometer (blue) at  $B = -0.15$  G. Red and blue arrows mark the resonances corresponding to the same arrows in (B). Red curve is shifted vertically by 1 k $\Omega$  for clarity. Colormaps are saturated to better highlight noninversion to inversion crossovers. These maps are generated by sweeping  $B$  and  $I_{dc}$  with step sizes of 0.05 G and 1 nA, respectively.

As we discussed earlier, the voltage-biased terminal in an Andreev interferometer is analogous to an RF source. We note that coupling a two-terminal JJ to an EM field results in constant voltage steps in the current-voltage characteristics, known as Shapiro steps. However, even without any external EM field, the AC Josephson effect in a voltage-biased JJ may generate an EM field; via coupling to the metallic enclosure of the cryostat, this may result in the formation of self-induced Shapiro-like steps [69] or Fiske resonances [70] in the  $R$  versus  $V$  curves. To distinguish between self-induced Shapiro steps and the phase-ARs, we fabricate and characterize a two-terminal JJ which is adjacent to our three-terminal Andreev interferometer.

Figures 3A and B show the differential resistance  $R$  as a function of the superconducting flux and bias voltage in a two-terminal JJ and three-terminal Andreev interferometer, respectively. The graphene channel of the two-terminal JJ is 1  $\mu$ m long and 0.5  $\mu$ m wide. We observe two additional resonances above the critical current in the two-terminal JJ when the voltage bias is within  $\pm 25 \mu$ V ( $|V_{bias}| \leq 25 \mu$ V). We attribute these resonances to self-induced Shapiro steps which are consistent with the transverse modes of our cylindrical enclosure [71]. In contrast to this control measurement, we observe two

additional dark-bright regions (red and blue arrows in Fig. 3B) in our Andreev interferometer: these fall outside of the bias voltage range for self-induced Shapiro steps. Therefore, we attribute these crossovers to phase-AR processes. Figure 3C shows vertical cuts of  $R$  versus  $V_{bias}$  (red curve) and  $V_{LT}$  (blue curve) at  $\Phi = -0.15$  G corresponding to vertical dashed lines in Figs. 3A and B, respectively. Red and blue arrows mark the resonances corresponding to the same arrows in Fig. 3B. We note that in the three-terminal Andreev interferometer, we still observe multiple crossovers for  $|V_{LT}| \leq 25\mu\text{V}$ . However, it is challenging to identify whether these crossovers correspond to self-induced Shapiro steps or phase-ARs as both processes lead to similar signatures in  $R$  versus  $\varphi$  data.

In conclusion, we studied nonequilibrium Andreev resonances in a voltage-biased three-terminal graphene Andreev interferometer. We observed periodic resonances in the differential resistance  $R$  versus  $\varphi$ , which we attributed to the energy-phase relation of the ABSs. More specifically, we observed crossovers of these resonances to an inversion regime, that is,  $R$  is larger at multiples of half-flux quantum instead of flux quantum, with an applied bias voltage. To understand the microscopic mechanisms of noninversion to inversion crossovers, we developed a theoretical model based on the interplay of the static ABSs and the nonequilibrium Fermi surface of graphene. This model considers a phase-sensitive AR mechanism that couples the normal and superfluid components of

the current. This coupling results in the exchange of Cooper pairs with unpaired electrons and consequently leads to noninversion to inversion crossovers. We further investigated the impact of self-induced Shapiro steps by comparing  $R$  versus  $\varphi$  resonances in two-terminal JJs and three-terminal Andreev interferometers. For the two-terminal JJ, we found resonances for  $|V_{bias}| \leq 25\mu\text{V}$ , whereas for the three-terminal Andreev interferometer, we observed resonance both within and above the  $25\mu\text{V}$  range. We finally concluded that both EM coupling to the cavity modes of the enclosure and phase-ARs produce similar signatures in  $R$  versus  $V$ . In future studies, we anticipate further elucidating this phase-AR mechanism and its correlation with the predicted Floquet-Andreev states in MTJJs using tunneling spectroscopy [72, 73] to reveal the density of states of ABSs.

The data supporting the conclusions of this letter is available on Zenodo [74].

## ACKNOWLEDGMENTS

A.S.R., N.S., and M.K. acknowledge the Pennsylvania State University Materials Research Science and Engineering Center supported by the US National Science Foundation (DMR 2011839). R.M. acknowledges support from the French CNRS in Grenoble and the German KIT in Karlsruhe, which is funded by the International Research Project SUPRADEV MAT.

- 
- [1] A. Furusaki and M. Tsukada, Current-carrying states in josephson junctions, *Phys. Rev. B* **43**, 10164 (1991).
  - [2] I. O. Kulik, Macroscopic quantization and the proximity effect in s-n-s junctions, *Soviet Journal of Experimental and Theoretical Physics* **30**, 944 (1969).
  - [3] C. Ishii, Josephson currents through junctions with normal metal barriers, *Progress of Theoretical Physics* **44**, 1525 (1970).
  - [4] P. F. Bagwell, Suppression of the josephson current through a narrow, mesoscopic, semiconductor channel by a single impurity, *Phys. Rev. B* **46**, 12573 (1992).
  - [5] J. A. Sauls, Andreev bound states and their signatures, *Philosophical Transactions of the Royal Society A: Mathematical, Physical and Engineering Sciences* **376**, 20180140 (2018).
  - [6] A. Zazunov, V. S. Shumeiko, E. N. Bratus', J. Lantz, and G. Wendin, Andreev level qubit, *Phys. Rev. Lett.* **90**, 087003 (2003).
  - [7] C. Padurariu and Y. V. Nazarov, Theoretical proposal for superconducting spin qubits, *Phys. Rev. B* **81**, 144519 (2010).
  - [8] M. Pita-Vidal, A. Bargerbos, R. Žitko, L. J. Splitthoff, L. Grünhaupt, J. J. Wesdorp, Y. Liu, L. P. Kouwenhoven, R. Aguado, B. van Heck, A. Kou, and C. K. Andersen, Direct manipulation of a superconducting spin qubit strongly coupled to a transmon qubit, *Nature Physics* **19**, 1110 (2023).
  - [9] N. M. Chtchelkatchev and Y. V. Nazarov, Andreev quantum dots for spin manipulation, *Phys. Rev. Lett.* **90**, 226806 (2003).
  - [10] D. Z. Haxell, M. Coraiola, D. Sabonis, M. Hinderling, S. C. ten Kate, E. Cheah, F. Krizek, R. Schott, W. Wegscheider, W. Belzig, J. C. Cuevas, and F. Nichele, Microwave-induced conductance replicas in hybrid josephson junctions without floquet-andreev states, *Nature Communications* **14**, 6798 (2023).
  - [11] J. J. A. Baselmans, A. F. Morpurgo, B. J. van Wees, and T. M. Klapwijk, Reversing the direction of the supercurrent in a controllable josephson junction, *Nature* **397**, 43 (1999).
  - [12] D. J. van Woerkom, A. Proutski, B. van Heck, D. Bouman, J. I. Väyrynen, L. I. Glazman, P. Krogstrup, J. Nygård, L. P. Kouwenhoven, and A. Geresdi, Microwave spectroscopy of spinful andreev bound states in ballistic semiconductor josephson junctions, *Nature Physics* **13**, 876 (2017).
  - [13] S. Park, W. Lee, S. Jang, Y.-B. Choi, J. Park, W. Jung, K. Watanabe, T. Taniguchi, G. Y. Cho, and G.-H. Lee, Steady floquet-andreev states in graphene josephson junctions, *Nature* **603**, 421 (2022).
  - [14] D. T. Liu, J. Shabani, and A. Mitra, Floquet majorana zero and  $\pi$  modes in planar josephson junctions, *Phys. Rev. B* **99**, 094303 (2019).
  - [15] D. J. Carrad, L. Stampfer, D. Olsteins, C. E. N. Petersen, S. A. Khan, P. Krogstrup, and T. S. Jespersen, Photon-assisted tunneling of high-order multiple andreev reflection

- tions in epitaxial nanowire josephson junctions, *Nano Letters* **22**, 6262 (2022), pMID: 35862144.
- [16] P. E. Dolgirev, M. S. Kalenkov, and A. D. Zaikin, Interplay between josephson and aharonov-bohm effects in andreev interferometers, *Scientific Reports* **9**, 1301 (2019).
  - [17] D. Margineda, J. S. Claydon, F. Qejvanaj, and C. Checkley, Observation of anomalous josephson effect in nonequilibrium andreev interferometers, *Phys. Rev. B* **107**, L100502 (2023).
  - [18] M. S. Crosser, J. Huang, F. Pierre, P. Virtanen, H. T. T., F. K. Wilhelm, and N. O. Birge, Nonequilibrium transport in mesoscopic multi-terminal josephson junctions, *Phys. Rev. B* **77**, 014528 (2008).
  - [19] J. S. Meyer and M. Houzet, Nontrivial chern numbers in three-terminal josephson junctions, *Phys. Rev. Lett.* **119**, 136807 (2017).
  - [20] E. V. Repin, Y. Chen, and Y. V. Nazarov, Topological properties of multiterminal superconducting nanostructures: Effect of a continuous spectrum, *Phys. Rev. B* **99**, 165414 (2019).
  - [21] L. Peralta Gavensky, G. Usaj, and C. A. Balseiro, Topological phase diagram of a three-terminal josephson junction: From the conventional to the majorana regime, *Phys. Rev. B* **100**, 014514 (2019).
  - [22] V. Chandrasekhar, Probing the topological band structure of diffusive multiterminal Josephson junction devices with conductance measurements, *Applied Physics Letters* **121**, 222601 (2022).
  - [23] R.-P. Riwar, M. Houzet, J. S. Meyer, and Y. V. Nazarov, Multi-terminal josephson junctions as topological matter, *Nature Communications* **7**, 11167 (2016).
  - [24] L. P. Gavensky, G. Usaj, and C. A. Balseiro, Multiterminal josephson junctions: A road to topological flux networks, *Europhysics Letters* **141**, 36001 (2023).
  - [25] R. Mélin, R. Danneau, and C. B. Winkelmann, Proposal for detecting the  $\pi$ -shifted cooper quartet supercurrent, *Phys. Rev. Res.* **5**, 033124 (2023).
  - [26] R. Mélin and D. Feinberg, Quantum interferometer for quartets in superconducting three-terminal josephson junctions, *Phys. Rev. B* **107**, L161405 (2023).
  - [27] T. Oka and S. Kitamura, Floquet engineering of quantum materials, *Annual Review of Condensed Matter Physics* **10**, 387 (2019).
  - [28] M. S. Rudner and N. H. Lindner, Band structure engineering and non-equilibrium dynamics in floquet topological insulators, *Nature Reviews Physics* **2**, 229 (2020).
  - [29] R. Mélin, J.-G. Caputo, K. Yang, and B. Douçot, Simple floquet-wannier-stark-andreev viewpoint and emergence of low-energy scales in a voltage-biased three-terminal josephson junction, *Phys. Rev. B* **95**, 085415 (2017).
  - [30] L. Peralta Gavensky, G. Usaj, D. Feinberg, and C. A. Balseiro, Berry curvature tomography and realization of topological haldane model in driven three-terminal josephson junctions, *Phys. Rev. B* **97**, 220505 (2018).
  - [31] R. Mélin, R. Danneau, K. Yang, J.-G. Caputo, and B. Douçot, Engineering the floquet spectrum of superconducting multiterminal quantum dots, *Phys. Rev. B* **100**, 035450 (2019).
  - [32] N. Pankratova, H. Lee, R. Kuzmin, K. Wickramasinghe, W. Mayer, J. Yuan, M. G. Vavilov, J. Shabani, and V. E. Manucharyan, Multiterminal josephson effect, *Phys. Rev. X* **10**, 031051 (2020).
  - [33] G. V. Graziano, J. S. Lee, M. Pendharkar, C. J. Palmstr, and V. S. Pribiag, Transport studies in a gate-tunable three-terminal josephson junction, *Phys. Rev. B* **101**, 054510 (2020).
  - [34] S. Matsuo, J. S. Lee, C.-Y. Chang, Y. Sato, K. Ueda, C. J. Palmström, and S. Tarucha, Observation of nonlocal josephson effect on double inas nanowires, *Communications Physics* **5**, 221 (2022).
  - [35] A. W. Draelos, M.-T. Wei, A. Seredinski, H. Li, Y. Mehta, K. Watanabe, T. Taniguchi, I. V. Borzenets, F. Amet, and G. Finkelstein, Supercurrent flow in multiterminal graphene josephson junctions, *Nano Letters* **19**, 1039 (2019).
  - [36] E. G. Arnault, T. F. Q. Larson, A. Seredinski, L. Zhao, S. Idris, A. McConnell, K. Watanabe, T. Taniguchi, I. Borzenets, F. Amet, and G. Finkelstein, Multiterminal inverse ac josephson effect, *Nano Letters* **21**, 9668 (2021), pMID: 34779633.
  - [37] E. Strambini, S. D'Ambrosio, F. Vischi, F. Bergeret, Y. V. Nazarov, and F. Giazotto, The  $\omega$ -squeezing as a tool to phase-engineer josephson topological materials, *Nature Nanotechnology* **11**, 1055 (2016).
  - [38] A. H. Pfeffer, J. E. Duvauchelle, H. Courtois, R. Mélin, D. Feinberg, and F. Lefloch, Subgap structure in the conductance of a three-terminal josephson junction, *Phys. Rev. B* **90**, 075401 (2014).
  - [39] E. G. Arnault, S. Idris, A. McConnell, L. Zhao, T. F. Larson, K. Watanabe, T. Taniguchi, G. Finkelstein, and F. Amet, Dynamical stabilization of multiplet supercurrents in multiterminal josephson junctions, *Nano Letters* **22**, 7073 (2022), pMID: 35997531.
  - [40] G. V. Graziano, M. Gupta, M. Pendharkar, J. T. Dong, C. P. Dempsey, C. Palmström, and V. S. Pribiag, Selective control of conductance modes in multiterminal josephson junctions, *Nature Communications* **13**, 10.1038/s41467-022-33682-2 (2022).
  - [41] F. Zhang, A. S. Rashid, M. T. Ahari, W. Zhang, K. M. Ananthanarayanan, R. Xiao, G. J. de Coster, M. J. Gilbert, N. Samarth, and M. Kayyalha, Andreev processes in mesoscopic multiterminal graphene josephson junctions, *Phys. Rev. B* **107**, L140503 (2023).
  - [42] Y. Cohen, Y. Ronen, J.-H. Kang, M. Heiblum, D. Feinberg, R. Mélin, and H. Shtrikman, Nonlocal supercurrent of quartets in a three-terminal josephson junction, *Proceedings of the National Academy of Sciences* **115**, 6991 (2018).
  - [43] M. Gupta, V. Khade, C. Riggert, L. Shani, G. Menning, P. Lueb, J. Jung, R. Mélin, E. P. A. M. Bakkers, and V. S. Pribiag, Evidence for  $\pi$ -shifted cooper quartets and few-mode transport in pbte nanowire three-terminal josephson junctions (2024), [arXiv:2312.17703](https://arxiv.org/abs/2312.17703) [cond-mat.mes-hall].
  - [44] J. Pillet, V. Benzoni, J. Griesmar, J.-L. Smir, and C. O. Girit, Nonlocal josephson effect in andreev molecules, *Nano Letters* **19**, 7138 (2019).
  - [45] M. Coraiola, D. Z. Haxell, D. Sabonis, H. Weisbrich, A. E. Svetogorov, M. Hinderling, S. C. ten Kate, E. Cheah, F. Krizek, R. Schott, W. Wegscheider, J. C. Cuevas, W. Belzig, and F. Nichele, Phase-engineering the andreev band structure of a three-terminal josephson junction, *Nature Communications* **14**, 6784 (2023).
  - [46] S. Matsuo, T. Imoto, T. Yokoyama, Y. Sato, T. Lindemann, S. Gronin, G. C. Gardner, S. Nakosai, Y. Tanaka, M. J. Manfra, and S. Tarucha, Phase-dependent andreev molecules and superconducting gap closing in coherently-coupled josephson junctions, *Nature Communications*

- 14, 8271 (2023).
- [47] S. Matsuo, T. Imoto, T. Yokoyama, Y. Sato, T. Lindemann, S. Gronin, G. C. Gardner, M. J. Manfra, and S. Tarucha, Phase engineering of anomalous josephson effect derived from andreev molecules, *Science Advances* **9**, eadj3698 (2023).
  - [48] M. Coraiola, D. Z. Haxell, D. Sabonis, M. Hinderling, S. C. ten Kate, E. Cheah, F. Krizek, R. Schott, W. Wegscheider, and F. Nichele, Spin-degeneracy breaking and parity transitions in three-terminal josephson junctions (2023), [arXiv:2307.06715 \[cond-mat.mes-hall\]](#).
  - [49] M. Gupta, G. V. Graziano, M. Pendharkar, J. T. Dong, C. P. Dempsey, C. Palmstrøm, and V. S. Pribiag, Gate-tunable superconducting diode effect in a three-terminal josephson device, *Nature Communications* **14**, 3078 (2023).
  - [50] M. Coraiola, A. E. Svetogorov, D. Z. Haxell, D. Sabonis, M. Hinderling, S. C. ten Kate, E. Cheah, F. Krizek, R. Schott, W. Wegscheider, J. C. Cuevas, W. Belzig, and F. Nichele, Flux-tunable josephson diode effect in a hybrid four-terminal josephson junction, *ACS Nano* **18**, 9221 (2024), pMID: 38488287.
  - [51] J. Chiles, E. G. Arnault, C.-C. Chen, T. F. Q. Larson, L. Zhao, K. Watanabe, T. Taniguchi, F. Amet, and G. Finkelstein, Nonreciprocal supercurrents in a field-free graphene josephson triode, *Nano Letters* **23**, 5257 (2023), pMID: 37191404.
  - [52] F. Zhang, A. S. Rashid, M. Tanhayi Ahari, G. J. de Coster, T. Taniguchi, K. Watanabe, M. J. Gilbert, N. Samarth, and M. Kayyalha, Magnetic-field-free non-reciprocal transport in graphene multiterminal josephson junctions, *Phys. Rev. Appl.* **21**, 034011 (2024).
  - [53] S. Matsuo, T. Imoto, T. Yokoyama, Y. Sato, T. Lindemann, S. Gronin, G. C. Gardner, M. J. Manfra, and S. Tarucha, Josephson diode effect derived from short-range coherent coupling, *Nature Physics* **19**, 1636 (2023).
  - [54] K.-F. Huang, Y. Ronen, R. Mélin, D. Feinberg, K. Watanabe, T. Taniguchi, and P. Kim, Evidence for  $4e$  charge of cooper quartets in a biased multi-terminal graphene-based josephson junction, *Nature Communications* **13**, 3032 (2022).
  - [55] R. Mélin and B. Douçot, Inversion in a four-terminal superconducting device on the quartet line. ii. quantum dot and floquet theory, *Phys. Rev. B* **102**, 245436 (2020).
  - [56] R. Mélin, Inversion in a four-terminal superconducting device on the quartet line. i. two-dimensional metal and the quartet beam splitter, *Phys. Rev. B* **102**, 245435 (2020).
  - [57] T. E. Golikova, M. J. Wolf, D. Beckmann, I. E. Batov, I. V. Bobkova, A. M. Bobkov, and V. V. Ryazanov, Nonlocal supercurrent in mesoscopic multiterminal sns josephson junction in the low-temperature limit, *Phys. Rev. B* **89**, 104507 (2014).
  - [58] R. Mélin, A. S. Rashid, and M. Kayyalha, Ultraclean andreev interferometers (2024), [arXiv:2403.13669 \[cond-mat.mes-hall\]](#).
  - [59] R. C. Dynes, V. Narayanamurti, and J. P. Garno, Direct measurement of quasiparticle-lifetime broadening in a strong-coupled superconductor, *Phys. Rev. Lett.* **41**, 1509 (1978).
  - [60] F. Jaworski, W. H. Parker, and S. B. Kaplan, Quasiparticle and phonon lifetimes in superconducting pb films, *Phys. Rev. B* **14**, 4209 (1976).
  - [61] F. J. Matute-Cañadas, L. Tosi, and A. L. Yeyati, Quantum circuits with multiterminal josephson-andreev junctions (2023), [arXiv:2312.17305 \[cond-mat.mes-hall\]](#).
  - [62] E. C. Gingrich, B. M. Niedzielski, J. A. Glick, Y. Wang, D. L. Miller, R. Loloee, W. P. Pratt Jr, and N. O. Birge, Controllable  $0-\pi$  josephson junctions containing a ferromagnetic spin valve, *Nature Physics* **12**, 564 (2016).
  - [63] T. Yamashita, K. Tanikawa, S. Takahashi, and S. Maekawa, Superconducting  $\pi$  qubit with a ferromagnetic josephson junction, *Phys. Rev. Lett.* **95**, 097001 (2005).
  - [64] L. Wang, I. Meric, P. Huang, Q. Gao, Y. Gao, H. Tran, T. Taniguchi, K. Watanabe, L. Campos, D. Muller, *et al.*, One-dimensional electrical contact to a two-dimensional material, *Science* **342**, 614 (2013).
  - [65] M. Tomi, M. R. Samatov, A. S. Vasenko, A. Laitinen, P. Hakonen, and D. S. Golubev, Joule heating effects in high-transparency josephson junctions, *Phys. Rev. B* **104**, 134513 (2021).
  - [66] I. V. Borzenets, F. Amet, C. T. Ke, A. W. Draelos, M. T. Wei, A. Seredinski, K. Watanabe, T. Taniguchi, Y. Bomze, M. Yamamoto, S. Tarucha, and G. Finkelstein, Ballistic graphene josephson junctions from the short to the long junction regimes, *Phys. Rev. Lett.* **117**, 237002 (2016).
  - [67] J. Knoch, Z. Chen, and J. Appenzeller, Properties of metal-graphene contacts, *IEEE Transactions on Nanotechnology* **11**, 513 (2012).
  - [68] P. E. Dolgirev, M. S. Kalenkov, A. E. Tarkhov, and A. D. Zaikin, Phase-coherent electron transport in asymmetric crosslike andreev interferometers, *Phys. Rev. B* **100**, 054511 (2019).
  - [69] T. M. Klapwijk and J. E. Sepers, M. and Mooij, Regimes in the behavior of superconducting microbridges, *Journal of Low Temperature Physics* **138**, 801 (1977).
  - [70] D. D. Coon and M. D. Fiske, Josephson ac and step structure in the supercurrent tunneling characteristic, *Phys. Rev.* **138**, A744 (1965).
  - [71] M. Popinciuc, V. E. Calado, X. L. Liu, A. R. Akhmerov, T. M. Klapwijk, and L. M. K. Vandersypen, Zero-bias conductance peak and josephson effect in graphene-nb junctions, *Phys. Rev. B* **85**, 205404 (2012).
  - [72] L. Bretheau, J. I.-J. Wang, R. Pisoni, K. Watanabe, T. Taniguchi, and P. Jarillo-Herrero, Tunneling spectroscopy of andreev states in graphene, *Nature Physics* **13**, 756 (2017).
  - [73] J. I.-J. Wang, L. Bretheau, D. Rodan-Legrain, R. Pisoni, K. Watanabe, T. Taniguchi, and P. Jarillo-Herrero, Tunneling spectroscopy of graphene nanodevices coupled to large-gap superconductors, *Phys. Rev. B* **98**, 121411 (2018).
  - [74] Nonequilibrium Andreev resonances in ultraclean graphene Andreev interferometers [Data set]. Zenodo.



## Supporting Information

### I. NONINVERSION TO INVERSION CROSSOVERS IN ANOTHER DEVICE

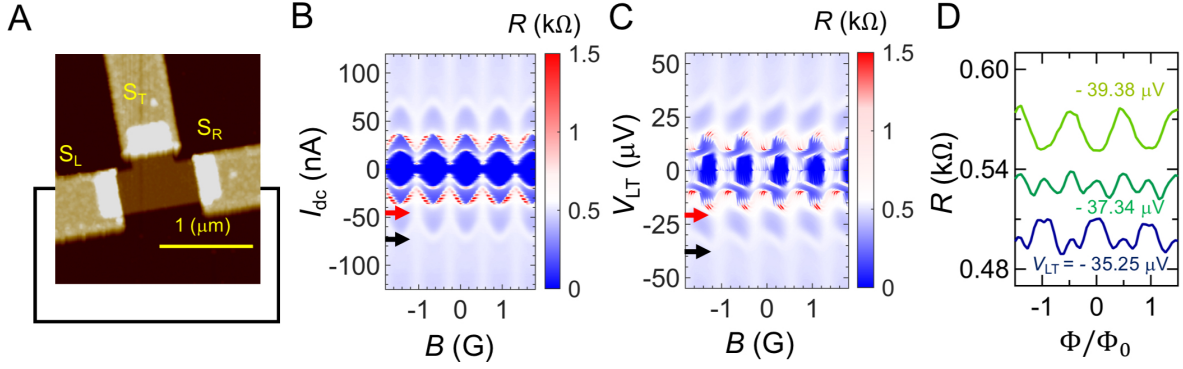


FIG. S1. (A) Atomic force microscope (AFM) image of another three-terminal Andreev interferometer. Unlike the device presented in the main text, this device does not have any tunneling probe. (B, C) Differential resistance  $R$  as a function of the magnetic field  $B$  and, respectively, bias current  $I_{dc}$  (B) and bias voltage  $V_{LT}$  (C) at  $V_g = 20$  V and  $T = 12$  mK. Arrows mark noninversion to inversion crossovers. (D) Differential resistance  $R$  as a function of the magnetic flux  $\Phi$  for the crossovers marked by the black arrows in (B) and (C). The oscillations show an evolution from maxima to minima with increasing  $V_{LT}$ . Curves are shifted vertically by 0.04 k $\Omega$  for clarity. Colormaps are saturated to better highlight noninversion to inversion crossovers. These maps are generated by sweeping  $B$  and  $I_{dc}$  with step sizes of 0.05 G and 1 nA, respectively.

### II. ADDITIONAL LINE CUTS OF DIFFERENTIAL RESISTANCE MAPS

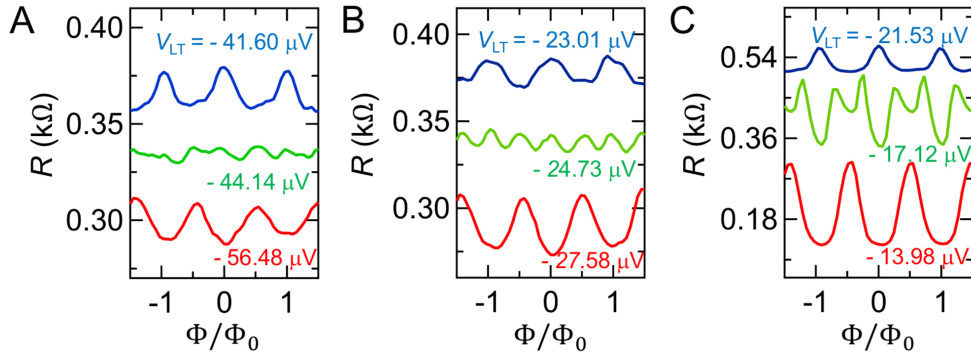


FIG. S2. (A-C) Differential resistance  $R$  as a function of the magnetic flux  $\Phi$  for the crossovers marked by the black (A), yellow (B), and purple (C) arrows in Figs. 1B and C of the main text. The oscillations show an evolution from maxima to minima with increasing  $V_{LT}$ . Curves are shifted vertically by 0.03 k $\Omega$  for clarity.



### III. TEMPERATURE DEPENDENCE OF THE DIFFERENTIAL RESISTANCE MAPS

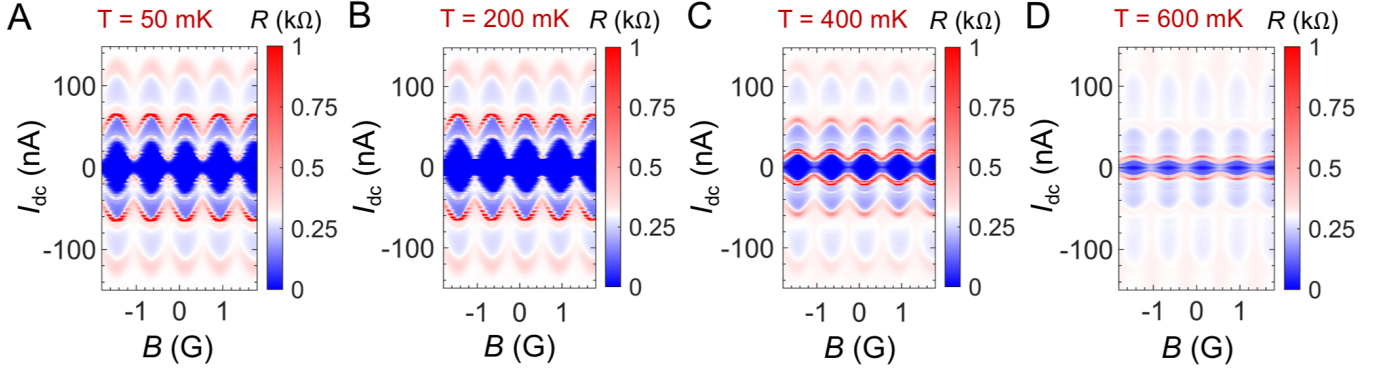


FIG. S3. (A-D) Temperature dependence of differential resistance  $R$  as a function of the magnetic field at 50 mK (A), 200 mK (B), 400 mK (C), and 600 mK (D). Colormaps are saturated to better highlight noninversion to inversion crossovers.

### IV. GATE VOLTAGE DEPENDENCE OF THE DIFFERENTIAL RESISTANCE MAPS

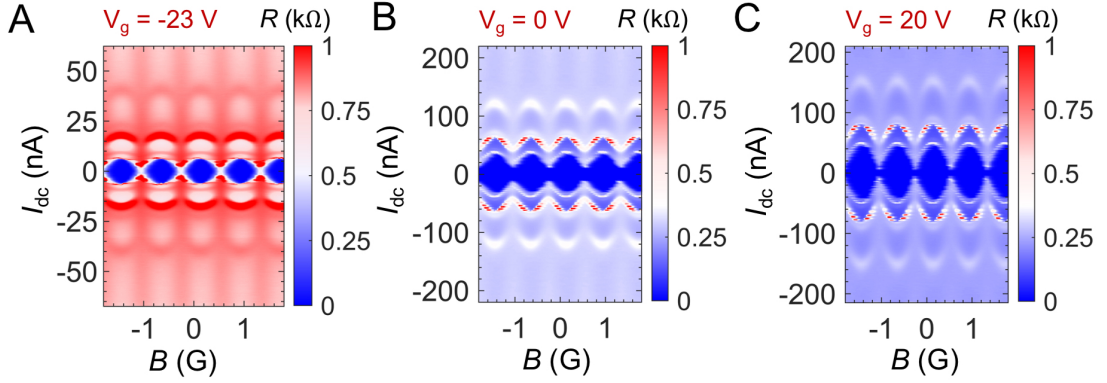


FIG. S4. (A-C) Differential resistance  $R$  as a function of the magnetic field at different gate voltages ( $V_g$ ) of -23 V (A), 0 V (B), and 20 V (C) at 12 mK. The Dirac point of graphene is at  $V_g = -12.5$  V. Colormaps are saturated to better highlight noninversion to inversion crossovers.